State-to-state exciton dynamics in semiconductor quantum dots

Samuel L. Sewall, Ryan R. Cooney, Kevin E. H. Anderson, Eva A. Dias, and Patanjali Kambhampati*
Department of Chemistry, McGill University, Montreal, QC, H3A 2K6, Canada
(Received 9 August 2006; revised manuscript received 12 October 2006; published 29 December 2006)

Femtosecond carrier relaxation dynamics in colloidal CdSe quantum dots are measured which focus on the early time dynamics for different initial excitonic states. Selecting the initial excitonic states produces a clear influence upon the early time dynamics. The difference between the dynamics when initially populating different excitonic states provides a direct measurement of excitonic relaxation times in strongly confined colloidal semiconductor quantum dots with specificity to electrons and holes. These results furthermore show state specific biexciton interactions.

DOI: 10.1103/PhysRevB.74.235328 PACS number(s): 78.47.+p, 73.21.La, 78.67.Hc

I. INTRODUCTION

Semiconductor quantum dots have a unique electronic structure that is between the limits of atomic and bulk size scales.[1] Spatial confinement of the charge carriers can result in size dependent electronic structure of the semiconductor. Quantum size effects can furthermore influence dynamical processes in these materials. Probing carrier relaxation dynamics in semiconductor quantum dots is important both for understanding the fundamental physics of nanoscale materials as well as for their incorporation into optoelectronic devices.[2,3]

Femtosecond laser spectroscopy has been a powerful tool in investigating the role of quantum confinement effects on relaxation processes in colloidal semiconductor quantum dots. These methods have been used to probe energy relaxation through the excited state manifold as well as many body interactions and population decay.[2–13] Femtosecond experiments have also been used to probe optical gain,[14] ionization dynamics,[15] carrier multiplication,[16] biexciton interactions,[2,6,17–24] and other dynamical processes.[25,26]

These spectroscopic experiments have provided critical tests of theories of carrier relaxation and recombination in quantum confined semiconductors as well as providing a foundation for incorporating these materials into optical devices.[3] While tremendous effort has been put toward elucidating electron and hole relaxation dynamics, a direct measure of electron and hole relaxation dynamics with state-to-state specificity has remained elusive due to the manifold of excitonic states produced by quantum confinement. We report here on the early time dynamics of excited carriers in semiconductor quantum dots with state-to-state specificity by spectroscopically selecting the initial excitonic state.

Semiconductor quantum dots have a size dependent level structure through quantum confinement of the electrons and holes.[27] Colloidal quantum dots are ideal for spectroscopic experiments since they are size tunable, allow strong confinement of the carriers, have well passivated surfaces, and have sufficient sample quality to observe atomiclike transitions.[28] Recent femtosecond pump-probe experiments on high quality colloidal quantum dots focused on ultrafast carrier relaxation dynamics with a fixed excitation wavelength, thus precluding specificity in the initial excitonic state for each size of particle.[2,5–7,10]

Since colloidal semiconductor quantum dots are size dependent, multi-electronic state systems further dressed with electronic fine structure, exciton selectivity combined with femtosecond time resolution should be promising towards a direct measure of dynamical processes in quantum confined semiconductors. We report here that the initial excitonic state in semiconductor quantum dots has a clear influence upon the early time femtosecond exciton relaxation dynamics. The initial state selective experiments reported here show (1) state-to-state relaxation dynamics of the electron in the presence of the hole, (2) state-to-state relaxation dynamics of the hole, and (3) state-specific biexciton interactions. An understanding of the early time state-to-state dynamics in quantum dots will be of benefit to more precise measurements of size dependent relaxation processes[29] and for probing excited states of biexcitons.[30]

II. BACKGROUND

An important feature in semiconductor quantum dots is the presence of atomiclike states for the exciton which arise from confinement.[27,31–33] This situation creates a spectroscopically resolvable eigenstate spectrum in which the electrons and holes may be characterized by envelope functions. Since there are specific excitonic eigenstates, there will also be state-to-state transition rates and state-to-state multiparticle Coulombic interactions. Selectivity in the initial and final states should facilitate observation of state-to-state exciton relaxation dynamics and multiparticle interactions.

Much work has been done on exciton relaxation mechanisms as a function of particle size.[2,3,5–7,9,10] Theory has predicted that there should be increased electron relaxation rates for hot excitons due to confinement enhanced Auger channels which circumvent the "phonon bottleneck."[34,35] The predicted rates for electron relaxation range from 0.1–2 ps, provided the hole is present as an acceptor channel. Experiments on high quality colloidal semiconductor quantum dots have been shown to corroborate confinement enhanced Auger relaxation channel for excitons, in which energy is unidirectionally transferred from the electron to the hole.[2,4,6,7,12,36,37] In this mechanism, electron relaxation is sub-picosecond due to the presence of the femtosecond Auger channel which is mediated by the hole.

In a related situation, experiments were performed on re-excited electrons with the Auger channel removed. These experiments show state-to-state electron relaxation on the 3–30 ps timescale when the hole is in a surface trapped state.[11–13] The slower electron relaxation times in these experiments is consistent with role of the femtosecond Auger channel mediated by the hole states of an exciton. When the hole is decoupled from the electron by spatial separation, the electron loses its femtosecond Auger channel. By using a sequential pumping scheme, the relaxation of the electron was directly measured with state specificity, in the absence of the hole induced femtosecond Auger channel. In the absence of the hole induced Auger channel, electron relaxation from the $1P$ state to the $1S$ state was directly measured to be on the 3–30 ps timescale.[11–13] It was moreover shown that the electron relaxation is strongly dependent upon the surface ligands,[11] thereby showing the importance of new relaxation pathways present in colloidal quantum dots.

A unified picture of electron relaxation should include all relevant processes such as phonon based relaxation, surface ligand induced relaxation, and hole induced Auger relaxation. Provided the hole remains coupled to the electron, the Auger channel will dominate electron relaxation. These experiments[2,6,11–13,37] have shown that there are at least two distinct mechanisms for electron relaxation in colloidal CdSe quantum dots in addition to the phonon based mechanisms found in bulk semiconductors. Furthermore, recent work by Klimov and co-workers has shown the presence of additional nonadiabatic relaxation channels in PbSe.[25] From these experiments it becomes clear that there are several pathways by which an excited exciton can relax. The total relaxation rate will be the sum of rates corresponding to each pathway, e.g., for electrons

$$k_{\text{total}} = k_{\text{Auger}} + k_{\text{surface}} + k_{\text{phonon}}. \quad (1)$$

The rate for a specific pathway contains the mechanistic information which is typically obtained from a Golden Rule based expression. Prior work has provided expressions for relaxation through emission of longitudinal optical (LO) phonons via the Fröhlich coupling,[2,6,38–40] electron to hole Auger processes,[34,35] interaction with surface ligands,[11] and nonadiabatic couplings mediated by LO phonons.[25] In the case of electron relaxation in CdSe quantum dots, the dominant pathway when the hole is present is the femtosecond Auger channel.

With the manifold of distinct relaxation pathways available in confined semiconductors, exciton relaxation dynamics merits further investigation with increased precision which focuses on the early time dynamics. Due the electronic structure of these quantum dots,[27,31,33] measurement relaxation dynamics with better than 100 fs precision have not been possible. Such precision is required in order to quantitatively measure timescales and establish a full picture of relaxation pathways. Sub-100 fs laser pulses alone will not solve the problem of obtaining precision measurement of exciton dynamics. Pumping at 3.1 eV with <50 fs pulses would still result in complex sequential dynamics requiring fitting to a many parameter model. Beyond time resolutions,

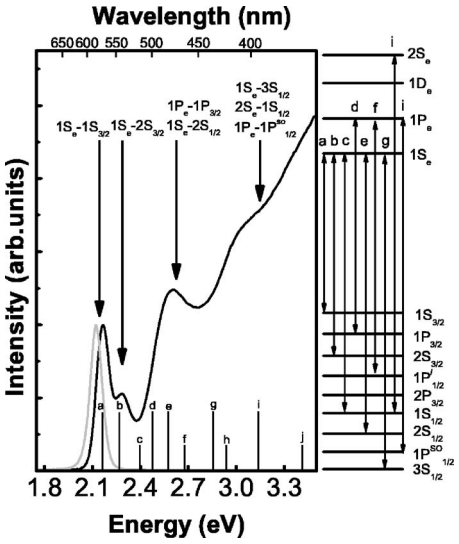

FIG. 1. Absorption spectrum of CdSe quantum dots (black line) and photoluminescence spectrum (grey line). The pump wavelengths and the initially prepared excitonic states are noted in the figure. The tall (short) sticks in the spectrum reflect high (low) oscillator strength transitions while the level diagram shows the transitions into specific excitonic states from Ref. 31. Assignments past transition *g* are ambiguous. Transitions which are both weak and ambiguous are not depicted in the level diagram.

spectral selectivity is important for precision measurements of state-to-state dynamics due to the excitonic state structure in quantum dots.

Additionally, the hole dynamics have not been directly measured for well-specified initial states. Prior work on hole dynamics used photoluminescence in conjunction with transient absorption to extract hole dynamics indirectly for arbitrary initial hole states.[7] Hole relaxation from different initial states to the ground state has directly been measured using a THz probe, however.[9] A precision measurement of relaxation dynamics of holes also requires selectivity in the initial excitonic state and the final excitonic state in order to precisely monitor the early time dynamics of the evolving exciton.

The electronic structure of colloidal semiconductor quantum dots may be characterized by envelope functions for the electron and the hole. A key point is that higher photon energy does not necessarily correspond to higher energy electrons[31] (see Fig. 1). The absorption spectrum can be decomposed into transitions corresponding to envelope functions for the electron and hole states.[27] The notation and positions for the stick spectrum are from published work on CdSe quantum dots.[31] First, higher energy transitions correspond to multiple electronic states due to higher density of states at higher energy.[31] More importantly, higher energy transitions may not necessarily create higher energy electronic states and would, therefore, not probe electron relaxation. The distribution of initial hot excitonic states created at high photon energy (e.g., $1S$, $1P$, $2S$), will sequentially populate lower energy states until the state corresponding to the probed transition is populated indirectly. Thus, the experimental transients reflect a sum of several processes convolved with the instrument response function, e.g.,

$$\Delta \mathrm{OD}(t) = \left(A_{1S} + A_{1P} e^{-k_1 t} + A_{2S} \times \left(1 + \frac{1}{k_2 - k_1} (k_1 e^{-k_2 t} - k_2 e^{-k_1 t}) \right) \right) \otimes \mathrm{IRF}. \quad (2)$$

The A's reflect the probability of excitation into a specific initial exciton and the k's reflect the total transition rate which is the sum of multiple pathways. IRF represents the instrument response function measured by cross-correlation of the pump and probe pulses. Here, $k_2 \equiv k_{2S \to 1P}$ and $k_1 \equiv k_{1P \to 1S}$. Each k represents the total rate for a state-to-state transition which is comprised of several pathways which contain the desired dynamical information [Eq. (1)]. The measured transients will be a convolution of the IRF with the actual population dynamics. It would be difficult to precisely and unambiguously fit the measured data to such a function, particularly when the dynamical processes can occur on the same 100 fs timescale as the IRF. These five parameters will furthermore change with the particle size reflecting the distribution of initial excitonic states and the size dependent transition rates.

In order to precisely measure the electron or hole relaxation rates for a hot exciton, specificity in the preparation of the initial excitonic state is required. Specificity in the initial excitonic state reflects *state-to-state dynamics* of the excited carriers where the same initial is prepared and the same final state is monitored for any quantum dot. By measuring state-to-state transition rates, the mechanisms underlying these transitions can be rigorously established. Specificity in the initial excitonic state will also facilitate monitoring exciton specific multiparticle interactions.

III. EXPERIMENT

Samples of colloidal CdSe quantum dots were prepared using published procedures.[41] The samples had no apparent deep trap emission and had absorption and emission linewidths characteristic of an ensemble dispersity of $\sigma < 10\%$. The present work focuses on CdSe with an energy gap of 2.17 eV, and a corresponding radius of 1.8 nm.[42] Toluene, methanol, hexanes, and acetone were obtained from Fisher and used as received. All other chemicals were purchased from Aldrich and used as received. The steady-state absorption measurements were performed on a Varian Cary 300 UV/Visible spectrophotometer. The photoluminescence (PL) and photoluminescence excitation (PLE) spectra were measured on a Spex Fluromax-2 spectrofluorometer. For these measurements the nanocrystals were dissolved in toluene.

The spectroscopic measurements were made using an amplified Ti:sapphire laser system (800 nm, 70 fs, 1 kHz, 2.5 mJ; Coherent) in the pump/probe configuration. The probe pulse was derived from single filament white light continuum generated in a 2 mm sapphire crystal. The pump pulses were derived by frequency doubling the 800 nm fundamental beam in a 100 μm β-BaB_2O_4 crystal (BBO), or via optical parametric amplifiers (OPA). The OPA derived pulses were ~60 fs at 475, 540, and 580 nm. The pump wavelengths were tuned to specific initial excitonic states (Fig. 1). Pumping at 400 nm (3.1 eV) was done for comparison to prior work.

The continuum and OPA pulses were dispersion compensated by fused silica prism pairs. The instrument response function (IRF) was 110–130 fs over all wavelength combinations. The pulse durations and instrument response functions were measured by autocorrelation and cross correlation in 30 and 100 μm BBO crystals at the sample position. Autocorrelations were measured to ±100 ps to verify the absence of satellite pulses.

To facilitate precise comparisons of transients at different pump wavelengths, the 400 nm pump experiments were performed *simultaneously* with an OPA pump experiment by alternately chopping each of the pumps beams such that there was shot to shot alternation of the pump color. Two transients were collected at 333 Hz, corresponding to pump/probe experiments at two different pump wavelengths. The frequencies and phases of the two choppers were set to produce a sequence of pump 1, no pump, pump 2. Gated integration was performed on each shot, which was then digitized at 18 bits. Probe ratiometry was performed after spectral selection in order to minimize effects of continuum noise. Pump normalization was performed for each laser shot to further minimize instrument drift and noise. Spot sizes were 300 μm (pump) and 50 μm (probe). Crossing angles were 5 degrees for both pump beams. The time delay between pulses was set by a computer controlled delay stage with 0.1 μm precision.

Prior work by Barbara and co-workers employed different pump wavelengths to spectroscopically select initial states[43–45] in molecular systems and to allow subtractive procedures to monitor early time relaxation processes related to excess energy.[44,45] These methods were extended here to include simultaneous measurement of transients at two pump wavelengths in order to minimize experimental variations due to instrument drift, sample variations, and sample aging.

The sample consisted of quantum dots dispersed in toluene and continuously circulated through a 1 mm path length quartz flow cell at room temperature. The pump fluence was set to maintain the same mean exciton occupancy, $\langle N \rangle = 0.5$.[2,36] The OD of the sample was 0.2. Bleach magnitudes were ~50 mOD at the band edge and noise levels were typically ~0.2 mOD. Step sizes were 10 fs for the first two ps. It was verified that there was no power dependence to the transients. Time constants were obtained by fitting the entire transient data to a model function consisting of a sum of exponentials convolved with the IRF. Three separate days of experiments were done on each of three different syntheses of the same size of quantum dot to ensure reproducibility of the results. Uncertainties in the fits were obtained by fitting at least ten transients for each day for each sample, resulting in standard deviations of ±15 fs.

IV. RESULTS AND DISCUSSION

A. Bleaching signals and electron dynamics

The early time dynamics of excited exciton is shown as a function of the initial excitonic state in Fig. 2. The transient at 570 nm probe arises from state filling induced bleaching

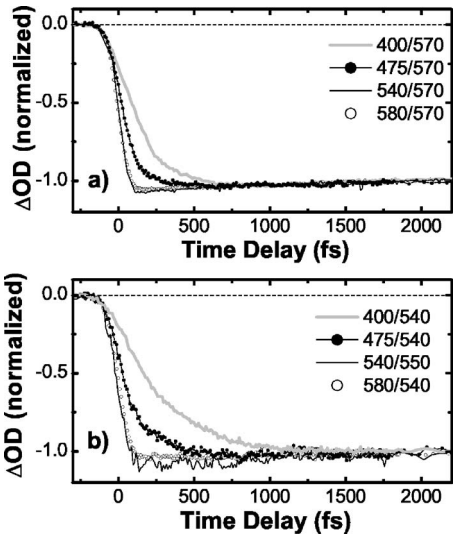

FIG. 2. Femtosecond pump-probe transients noted by pump/probe wavelengths. The transients have been normalized to the bleach at 2 ps. Each pump wavelengths correspond to different initial excitonic states as noted in Fig. 1. Higher energy pumping at 475 and 400 nm corresponds to multiple initial states due to an increased density of states at higher energy. Panel (a) corresponds to the band edge signal denoted $B1$ in Ref. 6. Panel (b) corresponds to the $B2$ feature.

of the $1S_e-1S_{3/2}$ transition, while the transient at 540 nm probe is primarily due to the $1S_e-2S_{3/2}$ transition.[2,6] These spectroscopic features are labeled $B1$ and $B2$, following the notation of Klimov and co-workers.[2,6] Figure 2(a) shows that pumping directly into the $1S_e-1S_{3/2}$ (580 nm) or the $1S_e-2S_{3/2}$ (540 nm) state produces the same instantaneous bleaching when probing a the $1S_e-1S_{3/2}$ band edge (570 nm). Figure 2(b) shows the identical results when probing at 540 nm. The slightly slower early time dynamics in Fig. 2(b) relative to Fig. 2(a) reproduces prior work by Klimov and co-workers,[2,6] reflecting partial cancellation from overlapping transitions.

The relation between the bleaching signals and electron dynamics can be made by considering the excitations at these wavelengths. There are four permutations of excitonic states which can be monitored at these wavelength combinations, (see Fig. 3). In all four situations, the electron remains in its lowest energy $1S$ state. Under these spectroscopic conditions,

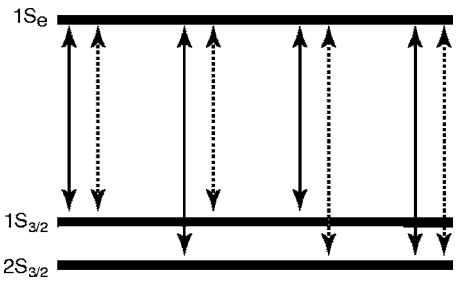

FIG. 3. Selected transitions relevant to evaluating state-to-state electron and hole dynamics. The solid line corresponds to the pumped transition and the dashed line corresponds to the probed transition.

the bleaching transients are independent of the hole state, Fig. 2. That two initial excitonic states produce the identical bleaching dynamics despite being in different hole states rigorously verifies prior assignment[2,6] that only electrons contribute to the bleaching signals due to the higher degeneracy of the valence band states. The early time dynamics obtained by exciton selectivity shows that the experimental bleaching signals only monitor the electron dynamics of the relaxing exciton.

In contrast to the instantaneous bleaching when initially populating $1S$ electrons, pumping into higher energy initial states at 475 and 400 nm results in buildup times to the band edge bleaching signals of 90 and 200 fs, respectively [Fig. 2(a)]. Pumping at 400 nm (3.1 eV) produces *multiple* initial excitonic states due to the increase density of states at higher energies. This distribution of initial states includes the $1S_e-3S_{3/2}$, $2S_e-1S_{1/2}$, $1P_e-1P^{SO}_{1/2}$ excitons [31] (Fig. 1). Other low oscillator strength states are likely to contribute as well.[31] Unlike the lower energy transitions, these higher excited states have ambiguities in their assignments.[31]

By spectroscopically selecting the initial excitonic state, the early time dynamics of hot electrons can be precisely monitored. The picosecond dynamics of the electrons are independent of the initial excitonic state, however. The 570 and 540 nm probe transients are identical past 2 ps for all initial excitonic states reported here. The 400 nm pump data reported here reproduces prior results at all probe wavelengths.[2,6,37] A key new result here is that excitons can be created in which electrons are directly prepared in the $1P$ state, which is reflected in the observed buildup time in the $1S$ bleaching feature.

While the bleaching features only monitor electron dynamics of the relaxing exciton, it is still not possible to precisely monitor electron relaxation of the initially created exciton. The primary spectroscopic difficulty arises from overlapping transitions and sequential transitions. Spectroscopic pumping will produce a distribution of excitons for which the electrons may be in states such as $1S+1P$, $1P+2S$, or $1S+1P+2S$. While pumping at 475 nm does reflect only electron relaxation, it does not directly monitor relaxation from the $1P$ state to the $1S$ state. Pumping at 400 nm (3.1 eV) will furthermore produce electrons in a $2S$ and several other states. In this case, the signals will reflect sequential dynamics and the measured time constants will not directly reflect the transitions of interest. The measured dynamics in principle reflect a sum of several processes which should be modeled as step functions, exponentials, and nonexponentials. The parameters of such a model would, furthermore, be size dependent. Thus, the time constants for pumping at 475 or 400 nm do not directly reflect electron relaxation from $1P$ to $1S$ with state-to-state specificity. These state-to-state electron dynamics can still be obtained with femtosecond precision by using subtractive procedures discussed in Sec. IV C.

B. Induced absorptions and hole dynamics

While the bleaching features directly reflect electron dynamics, the absorptive features can be used to probe hole

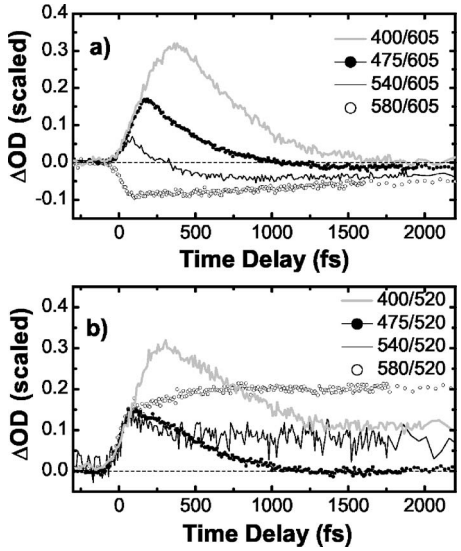

FIG. 4. Femtosecond pump-probe transients noted by pump/probe wavelengths. The transients have been scaled to the band edge bleach at the corresponding pump wavelength, reflecting the mean exciton occupancy, $\langle N \rangle$. The pump wavelengths correspond to different initial states as noted in Fig. 1. Higher energy pumping at 475 and 400 nm corresponds to multiple initial states due to an increased density of states at higher energy. Panel (a) corresponds to the induced absorption, denoted $A1$ in Ref. 6. Panel (b) corresponds to the $A2$ feature.

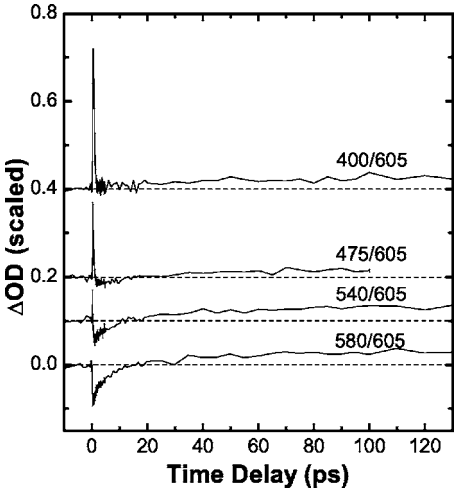

FIG. 5. Long time scan of the $A1$ feature illustrating the presence of up to four time scales of processes. The pump-probe transients are noted by pump/probe wavelengths.

dynamics of the relaxing exciton. The induced absorptions have been assigned to biexciton interactions rather than excited state absorption.[2,4,6] The known excited state absorptions are due to intraband transitions from 2000–5000 nm.[2,10,36,46] In agreement with previous results, no induced absorptions were observed from 650–800 nm. The only induced absorptions observed were visible at 605 and 520 nm, in agreement with previous results.[2,6,37] The observation of induced absorptions only immediately to the red or blue of the interband transitions is consistent with previous assignments that these features arise from biexciton processes rather than excited state absorption.

Exciton selective dynamics to the red of the band edge are shown in Fig. 4(a). Reflecting the exciton occupancy, $\langle N \rangle$, these transients have been scaled to the magnitude of the $1S$ bleaching transient at 2 ps at which point relaxation of the exciton to the band edge is complete. These pump wavelength dependent data show an instantaneous (IRF limited) bleach at 580/605, and an instantaneous induced absorption at 540/605 which decays into a bleach. At both these pump wavelengths the electron is in the same $1S$ state, whereas the hole state changes from $1S_{3/2}$ to $2S_{3/2}$ (Figs. 1 and 3). While the 580 pump data shows no apparent induced absorption, the 540 nm pump produces a hot hole which can induces a shift of the lowest energy $1S_e-1S_{3/2}$ state. Thus the transient absorption at 605 nm directly reflects differences in the hole state under these spectroscopic conditions.

The induced absorptions are labeled $A1$ and $A2$, using the notation of Klimov and co-workers.[2,6] Both the $A1$ and the $A2$ features show a strong dependence of the early time dynamics on the initial excitonic state. The $A1$ feature is of particular utility for monitoring relaxation dynamics since it is not overlapping with absorptive regions of the quantum dot spectrum. Focusing on the $A1$ feature, one sees that specific excitons can be prepared and monitored where only the hole state differs. The $A1$ feature furthermore shows the broad distribution of time scales present in these systems (Fig. 5). Up to four time scales are present in the $A1$ transient, ranging from ~100 fs to 100 ps. The transients are all identical by ~60 ps reflecting the point that the final state is independent of the initial state. We use the $A1$ feature to focus on the early time dynamics revealing state-to-state hole transitions. Pumping into the $1S_e-2S_{3/2}$ exciton still does not directly track hole relaxation. The $A1$ signal decays on a ~1 ps timescale even when pumping into the ground state $1S_e-1S_{3/2}$ exciton. State-to-state hole dynamics with femtosecond precision can still be obtained using exciton selectivity described below.

C. Electron and hole relaxation dynamics

Since pumping at higher photon energy produces multiple initial excitonic states, a subtractive method is required to directly monitor the population of P state electrons. The full level structure[27,31] shows that 475 nm pumping will produce a mixture of excitons in the $1P_e-1P_{3/2}$ and $1S_e-2S_{1/2}$ states (Fig. 1). The S-type transition at 475 nm will contribute the $1S$ bleaching signal as an instrument response limited bleach. In order to isolate the buildup time directly from depopulation of the $1P$ electronic state, we introduce the difference between the 475/570 and the 580/570 transients as ΔΔOD [Fig. 6(a)].

This form of excess energy spectroscopy was previously performed on molecular systems by Barbara and co-workers.[45] It is the decay of the ΔΔOD transient which directly reflects the depopulation of the $1P$ state electrons,

$$\Delta\Delta\mathrm{OD}(t) = e^{-kt} \otimes \mathrm{IRF}. \tag{3}$$

Since the ΔΔOD transient directly monitors state-to-state transitions, the only parameter is the state-to-state transition

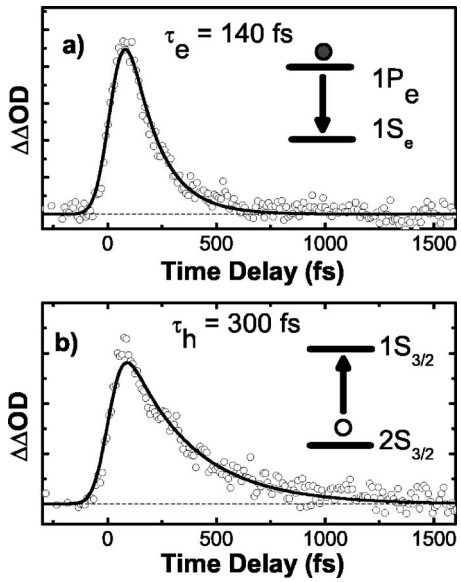

FIG. 6. State-to-state relaxation dynamics. The ΔΔOD transient is the subtraction of two ΔOD transients reflecting specific initial excitonic states chosen to reflect either electron or hole dynamics. Panel (a) shows the difference between the 475/570 and the 580/570 transients. Panel (b) shows the difference between the 540/605 and the 580/605 transients. The points are the data and the line is the fit.

rate, k. This direct method of extracting $1P$ electron dynamics is in contrast to a sequential kinetic model with multiple initial excitonic states, which would be necessary in the case of exciting at 400 nm into multiple highly excited states. From these direct measurements we assign an electron relaxation time from the $1P$ into the $1S$ state of 140 fs±15 fs. The corresponding energy relaxation rate for the $1P$ electron is 2.1 eV/ps. The time scales measured here show the importance of the Auger channel which is present upon creation of the initial hot exciton.

The difference between the transients for these two initial hole states offers a direct measure of the hole relaxation through the ΔΔOD transient. Figure 6(b) shows the difference between the transients which direct reflects population relaxation of the hole. From the initial state selectivity, we obtain a direct measure of the hole relaxation from $2S_{3/2}$ to $1S_{3/2}$ of 300 fs±15 fs. The corresponding energy relaxation rate for this initial hole state is 0.4 eV/ps. This result for the final stage of hole relaxation is more than twice as fast as the results of femtosecond photoluminescence measurements which lack state specificity,[7] but well matches recent time resolved THz experiments which directly measure arrival times of hot holes a well specified final state.[9] In contrast, these measurements on hole relaxation dynamics represent state-to-state measurements.

D. Biexciton interactions

In addition to directly monitoring carrier relaxation dynamics, these initial state dependent experiments reveal previously unobserved exciton state specific biexciton interactions. Biexcitons in quantum dots show increased binding

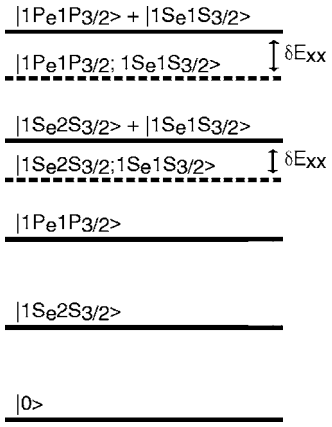

FIG. 7. Illustration of state specific biexciton interactions for two initial hot excitonic states, $1S_e-2S_{3/2}$, and $1P_e-1P_{3/2}$. Excited single exciton states are created by the pump pulse. Biexciton interactions with the $1S_e-1S_{3/2}$ exciton are monitored by timing the probe pulse prior to relaxation of the initial exciton. The biexiton binding energy, δE_{XX}, is specific to the four-particle system.

energies relative to the bulk phase.[4,19–24,46,47] Previous reports suggested that the biexciton Coulombic interaction manifests itself as an instantaneous induced absorption, as opposed to state filling which can have buildup times.[2,6,37] These signatures arise from Coulomb many body interactions. Prior work assigned the induced absorptions to carrier induced Stark processes by showing that the time zero transient absorption spectrum qualitatively matches the second derivative of the absorption spectrum[2] as well as the Stark spectrum due to external fields.[48–50] These redshifted transitions are more recently taken as signatures of biexcitons.[4,17,19–24,47,51–54]

Preparation of specific initial states is one way to probe whether different excitonic states produce different biexciton interactions. The induced absorption at 605 nm probe [Fig. 4(a)] shows clear differences due to the initial excitonic state. The induced absorption at lower photon energy arises from the initially created $1S_e-2S_{3/2}$ exciton (540 nm pump), inducing a shift of the lowest $1S_e-1S_{3/2}$ state through Coulombic multiparticle interaction (Fig. 7).

The most prominent effect occurs with excitation into the higher energy states at 475 and 400 nm [Fig. 4(a)]. Pumping at 475 nm initially populates $1P_e-1P_{3/2}$ and the $1S_e-2S_{1/2}$ excitons, while pumping at 400 nm produces a distribution of initial excitons (Fig. 1). Both these transients show buildup times of 200 fs and are dramatically different in amplitude when normalized to the mean exciton occupancy, $\langle N\rangle$. The differences between these two transients suggests that as the excitation relaxes through the manifold of states, specific excitonic states are transiently populated which result in state specific biexciton interactions (Fig. 7). The magnitude of the biexciton induced absorption reflects the magnitude of the biexciton binding energy, e.g., $|1P_e1P_{3/2}; 1S_e1S_{3/2}\rangle$ versus $|1S_e2S_{3/2}; 1S_e1S_{3/2}\rangle$.

Notably, these data show strong induced absorption signals even after 500 fs [Fig. 4(a)], at which point the electron is very nearly fully relaxed to the $1S$ state [Fig. 2(a)]. The differences in the absorptive transient at >500 fs are due to

the still relaxing hole producing state specific biexciton interactions—i.e., excited states of the biexciton. Figure 5 shows ps dynamics which depend upon the initial excitonic state. The differences arise from partial cancellation of state filling induced bleaching signals and biexciton related induced absorptive signals by the evolving distribution of excitonic states. Finally, the transients at 605 nm probe all become positive on the 50 ps time scale, due to the trapped carrier Stark effect.[2,6,55] That the signals all go to the same final positive offset indicates that the same final state is reached independent of the initial excitonic state. By monitoring the magnitude and evolution of the biexcitonic induced absorption, state specific biexcitonic interactions become apparent.

V. CONCLUSIONS

We report on the early time state-to-state exciton dynamics in high quality CdSe quantum dots as a function of the initial excitonic state. These early time dynamics were used to monitor both exciton relaxation dynamics and biexciton interactions with state specificity. Exciton selectivity allowed for monitoring state-to-state dynamics corresponding to either electron relaxation or hole relaxation with well defined initial and final states.

While femtosecond time resolution of laser pulses is important for precisely measuring exciton dynamics in quantum dots, the key point for increased precision in obtaining state specific dynamics is selectivity of the initial excitonic state. Relaxation of the hot electron was measured with 15 fs precision, under conditions where the ultrafast Auger channel is present. Relaxation of the hot hole was directly measured for the first time for a specific state-to-state transition. Specifically, these experiments yield the time for electron relaxation time from the $1P$ to the $1S$ state, and, the hole relaxation from the $2S_{3/2}$ to the $1S_{3/2}$ state. These experiments furthermore show evidence of state specific biexciton interactions representing excited states of the biexciton. The results obtained on state-to-state exciton dynamics will be extended for precision state-to-state measurements of the size dependence of electron and hole relaxation[29] and also to probe in more detail the excited states of the biexciton.[30]

ACKNOWLEDGMENTS

Financial support from the CFI, NSERC, FQRNT, and McGill University is gratefully acknowledged. We thank the McGill University Center for Self-Assembled Chemical Structures for use of their facilities. S.L.S. gratefully acknowledges a James McPhee Fellowship. E.A.D. gratefully acknowledges a NSERC CGS-M Fellowship. S.W. Koch is acknowledged for helpful comments.

*Author to whom correspondence should be addressed. Electronic address: pat.kambhampati@mcgill.ca

[1] A. P. Alivisatos, J. Phys. Chem. **100**, 13226 (1996).
[2] V. I. Klimov, J. Phys. Chem. B **104**, 6112 (2000).
[3] A. J. Nozik, Annu. Rev. Phys. Chem. **52**, 193 (2001).
[4] U. Woggon, H. Giessen, F. Gindele, O. Wind, B. Fluegel, and N. Peyghambarian, Phys. Rev. B **54**, 17681 (1996).
[5] V. I. Klimov, A. A. Mikhailovsky, D. W. McBranch, C. A. Leatherdale, and M. G. Bawendi, Science **287**, 1011 (2000).
[6] V. I. Klimov, D. W. McBranch, C. A. Leatherdale, and M. G. Bawendi, Phys. Rev. B **60**, 13740 (1999).
[7] S. Xu, A. A. Mikhailovsky, J. A. Hollingsworth, and V. I. Klimov, Phys. Rev. B **65**, 045319 (2002).
[8] D. F. Underwood, T. Kippeny, and S. J. Rosenthal, J. Phys. Chem. B **105**, 436 (2001).
[9] E. Hendry, M. Koeberg, F. Wang, H. Zhang, C. de Mello Donega, D. Vanmaekelbergh, and M. Bonn, Phys. Rev. Lett. **96**, 057408 (2006).
[10] C. Burda, S. Link, M. B. Mohamed, and M. El-Sayed, J. Chem. Phys. **116**, 3828 (2002).
[11] P. Guyot-Sionnest, B. Wehrenberg, and D. Yu, J. Chem. Phys. **123**, 074709 (2005).
[12] V. I. Klimov, A. A. Mikhailovsky, D. W. McBranch, C. A. Leatherdale, and M. G. Bawendi, Phys. Rev. B **61**, R13349 (2000).
[13] P. Guyot-Sionnest, M. Shim, C. Matranga, and M. Hines, Phys. Rev. B **60**, R2181 (1999).
[14] A. V. Malko, A. A. Mikhailovsky, M. A. Petruska, J. A. Hollingsworth, and V. I. Klimov, J. Phys. Chem. B **108**, 5250 (2004).
[15] D. H. Son, J. S. Wittenberg, and A. P. Alivisatos, Phys. Rev. Lett. **92**, 127406 (2004).
[16] R. D. Schaller and V. I. Klimov, Phys. Rev. Lett. **96**, 097402 (2006).
[17] V. Klimov, S. Hunsche, and H. Kurz, Phys. Rev. B **50**, 8110 (1994).
[18] F. Gindele, K. Hild, W. Langbein, and U. Woggon, Phys. Rev. B **60**, R2157 (1999).
[19] F. Gindele, U. Woggon, W. Langbein, J. M. Hvam, K. Leonardi, D. Hommel, and H. Selke, Phys. Rev. B **60**, 8773 (1999).
[20] B. Patton, W. Langbein, and U. Woggon, Phys. Rev. B **68**, 125316 (2003).
[21] Y. Z. Hu, S. W. Koch, M. Lindberg, N. Peyghambarian, E. L. Pollock, and F. F. Abraham, Phys. Rev. Lett. **64**, 1805 (1990).
[22] K. I. Kang, A. D. Kepner, S. V. Gaponenko, S. W. Koch, Y. Z. Hu, and N. Peyghambarian, Phys. Rev. B **48**, 15449 (1993).
[23] Y.-N. Hwang, K.-C. Je, D. Kim, and S.-H. Park, Phys. Rev. B **64**, 041305 (2001).
[24] U. Woggon, Springer Ser. Solid-State Sci. **146**, 107 (2004).
[25] R. D. Schaller, J. M. Pietryga, S. V. Goupalov, M. A. Petruska, S. A. Ivanov, and V. I. Klimov, Phys. Rev. Lett. **95**, 196401 (2005).
[26] C. Burda, S. Link, M. Mohamed, and M. El-Sayed, J. Phys. Chem. B **105**, 12286 (2001).
[27] A. L. Efros and M. Rosen, Annu. Rev. Phys. Chem. **30**, 475 (2000).
[28] C. B. Murray, D. J. Norris, and M. G. Bawendi, J. Am. Chem. Soc. **115**, 8706 (1993).

[29] R. R. Cooney, S. L. Sewall, E. D. Dias, D. M. Sagar, and P. Kambhampati (unpublished).
[30] S. L. Sewall, R. R. Cooney, D. M. Sagar, K. E. H. Anderson, and P. Kambhampati (unpublised).
[31] D. J. Norris and M. G. Bawendi, Phys. Rev. B **53**, 16338 (1996).
[32] D. J. Norris, A. L. Efros, M. Rosen, and M. G. Bawendi, Phys. Rev. B **53**, 16347 (1996).
[33] A. I. Ekimov, F. Hache, M. C. Schanne-Klein, D. Ricard, C. Flytzanis, I. A. Kudryavtsev, T. V. Yazeva, A. V. Rodina, and A. L. Efros, J. Opt. Soc. Am. B **10**, 100 (1993).
[34] A. L. Efros, V. A. Kharchenko, and M. Rosen, Solid State Commun. **93**, 281 (1995).
[35] L.-W. Wang, M. Califano, A. Zunger, and A. Franceschetti, Phys. Rev. Lett. **91**, 056404 (2003).
[36] V. I. Klimov, C. J. Schwarz, D. W. McBranch, C. A. Leatherdale, and M. G. Bawendi, Phys. Rev. B **60**, R2177 (1999).
[37] V. I. Klimov and D. W. McBranch, Phys. Rev. Lett. **80**, 4028 (1998).
[38] H. Benisty, C. M. Sotomayor-Torres, and C. Weisbuch, Phys. Rev. B **44**, 10945 (1991).
[39] U. Bockelmann and G. Bastard, Phys. Rev. B **42**, 8947 (1990).
[40] S. S. Prabhu, A. S. Vengurlekar, S. K. Roy, and J. Shah, Phys. Rev. B **51**, 14233 (1995).
[41] J. J. Li, Y. A. Wang, W. Guo, J. C. Keay, T. D. Mishima, M. B. Johnson, and X. Peng, J. Am. Chem. Soc. **125**, 12567 (2003).
[42] W. W. Yu, L. Qu, W. Guo, and X. Peng, Chem. Mater. **15**, 2854 (2003).
[43] P. Kambhampati, D. H. Son, T. W. Kee, and P. F. Barbara, J. Phys. Chem. A **106**, 2374 (2002).
[44] D. H. Son, P. Kambhampati, T. W. Kee, and P. F. Barbara, J. Phys. Chem. A **106**, 4591 (2002).
[45] P. Kambhampati, D.-H. Son, T. W. T. W. Kee, and P. F. Barbara, J. Phys. Chem. A **104**, 10637 (2000).
[46] C. Burda, S. Link, T. C. Green, and M. A. El-Sayed, J. Phys. Chem. B **103**, 10775 (1999).
[47] C. Burda and M. A. El-Sayed, Pure Appl. Chem. **72**, 165 (2000).
[48] V. L. Colvin and A. P. Alivisatos, J. Chem. Phys. **97**, 730 (1992).
[49] A. Sacra, D. J. Norris, C. B. Murray, and M. G. Bawendi, J. Chem. Phys. **103**, 5236 (1995).
[50] S. A. Empedocles and M. G. Bawendi, Science **278**, 2114 (1997).
[51] J. Y. Bigot, A. Daunois, J. Oberle, and J. C. Merle, Phys. Rev. Lett. **71**, 1820 (1993).
[52] M. Achermann, J. A. Hollingsworth, and V. I. Klimov, Phys. Rev. B **68**, 245302 (2003).
[53] A. A. Rogachev, Prog. Quantum Electron. **25**, 141 (2001).
[54] U. Woggon, K. Hild, F. Gindele, W. Langbein, M. Hetterich, M. Grun, and C. Klingshirn, Phys. Rev. B **61**, 12632 (2000).
[55] D. J. Norris, A. Sacra, C. B. Murray, and M. G. Bawendi, Phys. Rev. Lett. **72**, 2612 (1994).